Fabrication and Electrostatic Actuation of Thin Diaphragms

E. H. Yang*, S. S. Yang* and O. C. Jeong*

(Received June 5, 1995)

In this paper, two kinds of p^+ diaphragms are fabricated. One is flat, and the other is corrugated to release the residual stress resulted from the diffusion process. The two diaphragms are electrostatically actuated, and the center deflections of the diaphragms are measured for various frequencies. The static deflections of the flat diaphragm and the corrugated one estimated from the test results are compared with the calculated static deflections under residual tensile stress. The experimental result and the calculated result agree in the case of the flat diaphragm with a reasonable residual stress, but it is not true for the corrugated diaphragm. In the calculation, it is estimated that the corrugated diaphragm deflects more than the flat one. In the experiment, however, the corrugated diaphragm deflects less than the flat one.

Key Words: p^+ Diaphragm, Electrostatic Actuation, Residual Stress, Corrugated Diaphragm, Dynamic Testing, Damping

1. Introduction

Microactuators have been widely studied in recent years. The electrostatic actuator has advantages of the simple actuation over other actuators. In general, the electrostatic actuator is driven by the electrostatic attraction force between two parallel plates. In this paper, a p^+ silicon diaphragm is actuated with a fixed counter electrode. The p^+ silicon film is simply fabricated by the boron doped chemical etch stop method, and is useful for thin diaphragms. However, the tensile residual stress in the p^+ film reduces the deflection of the flat diaphragm against the pressure while the compressive residual stress causes buckling of the diaphragms.

One way to solve the problems of residual stresses is to fabricate the diaphragm corrugated for the stress release (Spiering *et al.*, 1991). For large corrugation depth (greater than 20μm), the deflection of the diaphragm is depending weakly on the residual stress and almost equals to that of the stress free diaphragm (Scheeper *et al.*, 1994). For the application of electrostatic actuator, however, large corrugation is not desirable because the attraction force of the electrostatic actuator is inversely proportional to the square of the distance between two electrodes. If there exists no residual stress, the corrugated diaphragm deflects more than the flat one in the large deflection region, and vice versa in the small deflection region (Jerman *et al.*, 1989; Mullem *et al.* 1991; Zhang and Wise, 1993; Scheeper *et al.*, 1994). If the residual stress is not negligible, the diaphragm behaviours are different from those of no residual stress. While the flat diaphragm deflects less due to tensile residual stress, the corrugated diaphragm is not so much affected by the residual stress (Scheeper *et al.*, 1994). Thus, the deflection of the flat diaphragm with tensile residual stress becomes smaller than that of the corrugated one in the small deflection region for large enough residual tensile stress. The static characteristics of the corrugated and the flat diaphragms under tensile residual stress have been investigated (Scheeper *et al.*, 1994; Hamberg *et al.*, 1995), but

* School of Electrical and Electronics Engineering AJOU University, 5 Wonchun-Dong, Suwon, 442-749, Korea
Tel: +82-331-219-2481, Fax: +82-331-212-9531

a dynamic test by electrostatic actuation has not been performed.

In this paper, an electrostatic actuator with a corrugated diaphragm and that with a flat one are fabricated for testing of the deflection characteristics in small deflection region under the residual stress. Their dynamic characteristics are tested and compared with the calculation results of static deflection under tensile residual stress, respectively.

2. Deflection by Electrostatic Actuation

Figures 1 and 2 illustrate the schematic view of actuators with the corrugated p^+ diaphragm and with the flat one, respectively. The p^+ diaphragms are moving electrodes and aluminum layer deposited on a #7740 pyrex glass is a fixed electrode. The diaphragms and electrodes are squares of the same dimension, a. In these figures, d_1 is the initial air gap of electrodes, d_2 is the thickness of the insulation layer, h is the thickness of the diaphragm, H is the corrugation depth, and l is the corrugation pitch.

When the voltage is applied to the counter electrodes of the actuators, the electrostatic force is generated between the electrodes. The diaphragms of the actuators are deflected by the attraction force. For the actuator with the flat electrode, the net electrostatic force, F is given by

$$F=\frac{1}{2}\left(\frac{\varepsilon_2(d_1-y)}{\varepsilon_2(d_1-y)+\varepsilon_1 d_2}\right)^2 \varepsilon_1 V^2 \frac{A}{(d_1-y)^2} \quad (1)$$

where A is the area of the electrode, y is the deflection of the diaphragm, and ε_1 and ε_2 are the permittivities of air and the insulator, respectively. V is the potential difference between the electrodes. In the case of the corrugated diaphragm, it is impossible to analytically derive the electrostatic force between the corrugated electrode and the flat one. For the approximate estimation of the force, the electrodes are regarded as parallel ones with the equivalent air gap. The equivalent air gap is determined by calculating the average distance between the aluminum layer and the corrugated diaphragm.

When one side of a flat diaphragm with a large initial stress is exposed to some pressure, the approximate relationship between the net applied

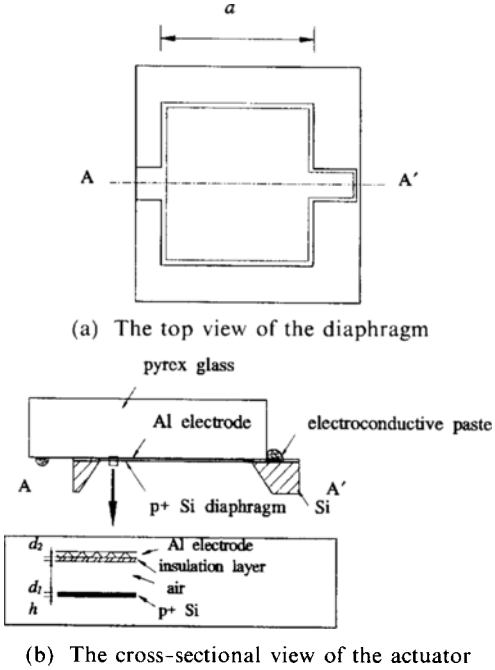

(a) The top view of the diaphragm

(b) The cross-sectional view of the actuator

Fig. 1 The schematic view of the electrostatic actuator with the flat diaphragm.

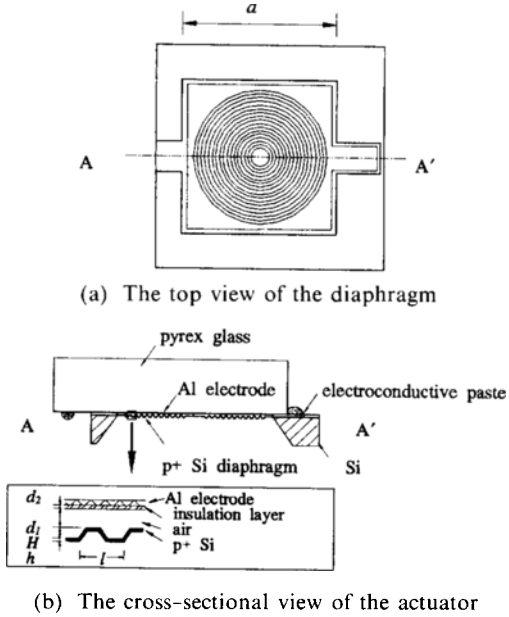

(a) The top view of the diaphragm

(b) The cross-sectional view of the actuator

Fig. 2 The schematic view of the electrostatic actuator with the corrugated diaphragm.

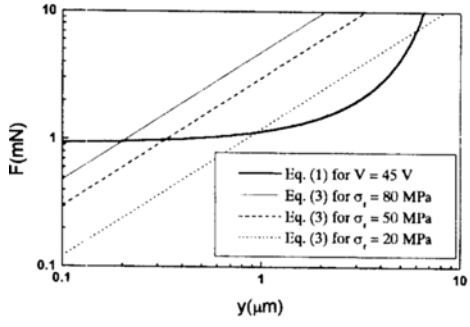

(a) $H=0$

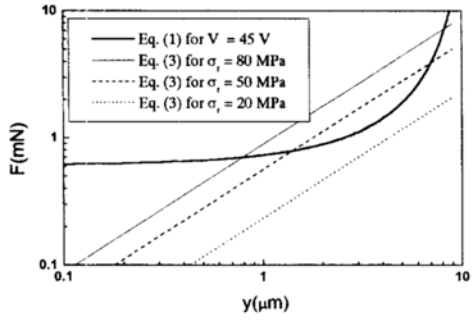

(b) $H=4\ \mu m$

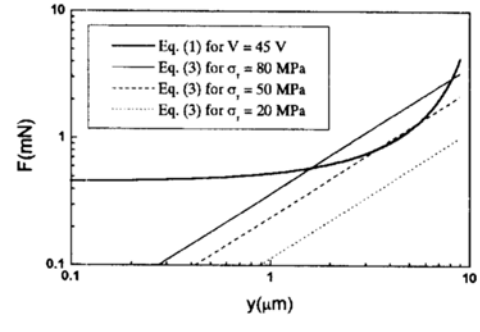

(c) $H=7\ \mu m$

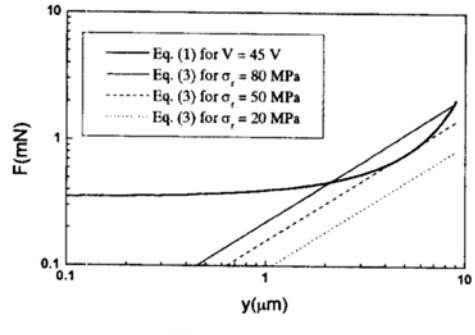

(d) $H=10\ \mu m$

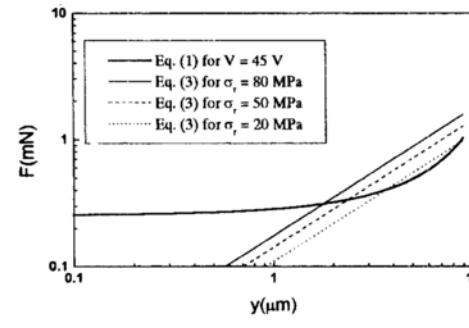

(e) $H=14\ \mu m$

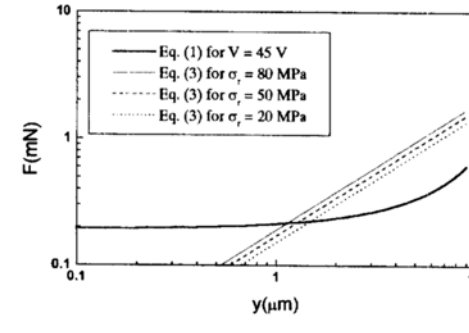

(f) $H=18\ \mu m$

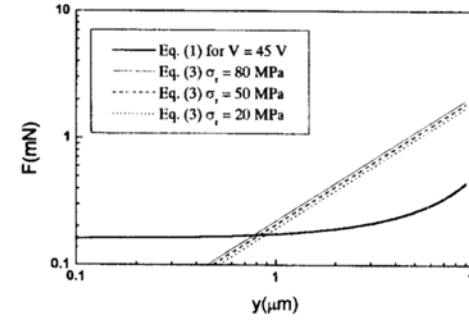

(g) $H=21\ \mu m$

Fig. 3 The center deflection of the diaphragm vs. the electrostatic force.

force, F and the static center deflection of the diaphragm, y under the residual stress, σ_r is given by (Scheeper *et al.*, 1994)

$$F=4\pi hy\left[\sigma_r+\frac{2.83}{4}\frac{E}{(1-\nu^2)}\frac{y^2}{r^2}\right] \quad (2)$$

where E, ν and r are Young's modulus, Poisson's ratio and an effective diaphragm radius, respectively. For the approximate calculations, the effective diaphragm radius, $r=a/\pi^{1/2}$ has been used (Scheeper *et al.*, 1994). The relationship between the net applied force and the static deflection of the circular corrugated diaphragm under a large initial stress for small deflection is (Scheeper *et al.*, 1994) as follows:

$$F=4\pi hy\left[\sigma_r\frac{B_p}{2.83}+\frac{A_p}{4}E\frac{h^2}{r^2}\right] \quad (3)$$

where A_p and B_p are

$$A_p=\frac{2(q+3)(q+1)}{3\left[1-\left(\frac{\nu}{q}\right)^2\right]}$$

$$B_p=32\frac{(1-\nu^2)}{(q^2-9)}\left[\frac{1}{6}-\frac{3-\nu}{(q-\nu)(q+3)}\right] \quad (4)$$

and q is the corrugation quality factor representing the corrugation geometry. For sinusoidal corrugation profiles, q is defined as

$$q^2=\frac{s}{l}\left[1+1.5\left(\frac{H}{h}\right)^2\right] \quad (5)$$

where s is the corrugation arc length. Figures 3 (a) ~ (g) show typical force-deflection curves of Eq. (3) for diaphragms with various corrugation depths and residual stresses when $E=122$ GPa and $\nu=0.25$. The dimensions of the diaphragm are arbitrarily set to $h=2$ μm, $r=1700$ μm, $d_1=9$ μm and $d_2=0.3$ μm in consideration of the fabrication feasibility. The curve of Eq. (1) represents the electrostatic force generated between electrodes when 45 V is applied. In the case of the corrugated diaphragm, it is impossible to analytically derive the electrostatic force between the corrugated electrode and the flat one. For the approximate estimation of the force, the electrodes are regarded as parallel ones with the equivalent air gap. The equivalent air gap is determined by calculating the average distance between the flat electrode and the corrugation

Table 1 The dimensions of the two electrostatic actuators.

(unit: μm)

	Flat	Corrugated
a	3000	3000
h	2	2
d_1	9	9
d_2	0.3	0.3
l		60
s		74
H		14

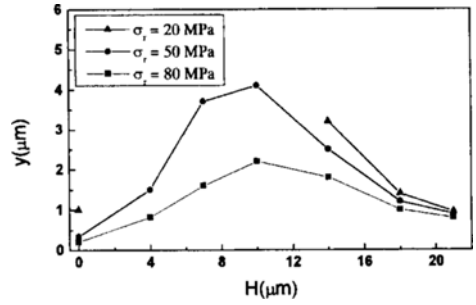

Fig. 4 The corrugation depth vs. the static deflection of the actuators.

profile of the diaphragm. In Figs. 3(a) ~ (g), the intersections of two curves indicate the equilibrium points of the static deflection. The lower point is the stable one and the upper point is the unstable one. Figure 3(a) shows the extreme case of $H=0$, that is, the flat diaphragm. As the corrugation becomes large, the effect of the residual stress decreases. Most of p^+ silicon films have the tensile residual stress of 10 to 100 MPa depending on the fabrication process (Maseeh and Senturia, 1989; Ding, Ko and Mansour, 1989; Ding and Ko, 1991; Wilner, 1992; Zhang and Wise, 1993; Yang and Yang, 1996). Figure 4 shows the stable static deflection of various corrugated diaphragms obtained from Figs. 3(a) ~ (g). It is obvious that in the case of the corrugated diaphragm with residual stress of 50 MPa or above, the diaphragm with the corrugation depth of 10 μm has the largest deflection. According to Fig. 3(d), however, there exist no stable equi-

librium point when the residual stress is less than 50 MPa. No stable equilibrium point means that the diaphragm stick to the fixed electrode. To avoid this stiction problem, it is perferable to fabricate a diaphragm with the corrugated depth of 14 μm. In Fig. 3(e), no stiction is expected if the residual stress is greater than about 10 MPa.

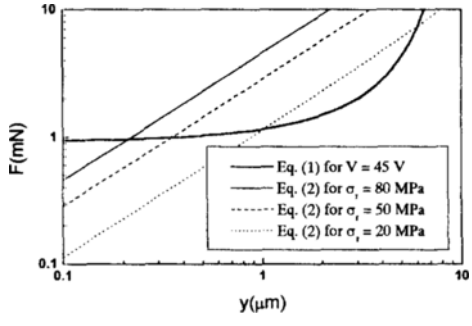

Fig. 5 The center deflection for the fabricated flat diaphragm vs. the electrostatic force.

From Fig. 4 the corrugated diaphragm with $H=$ 14 μm is estimated to deflect seven times as much as the flat diaphragm under residual stress of 50 MPa.

In this paper, two actuators with the dimensions represented in Table 1 are fabricated. In Fig. 4 the expected deflection of the corrugated diaphragm under the residual stress of 20 MPa is 3.2 μm. Figure 5 shows the curve of the electrostatic force when V=45 V, and the force-deflection curves of the flat diaphragm. The curves in Fig. 5 are the same as in Fig. 3(a) except that Eq. (2) has been used instead of Eq. (3) with $H=0$. The deflection of the flat diaphragm under the residual stress of 20 MPa obtained from Fig. 5 and Fig. 3(a) are 1.05 μm and 0.95 μm, respectively. The difference is due to the superpositon in the deduction of Eq. (3), the equation for the force-deflection relationship of the corrugated

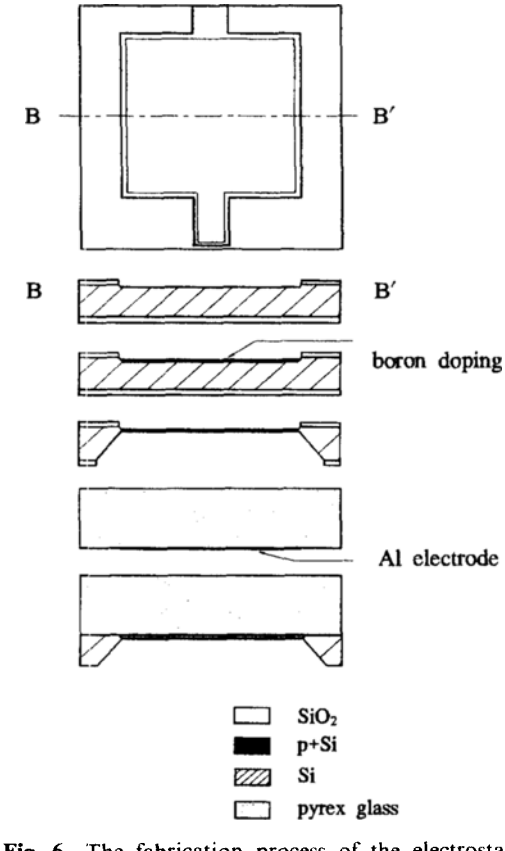

Fig. 6 The fabrication process of the electrostatic actuator with the flat diaphragm.

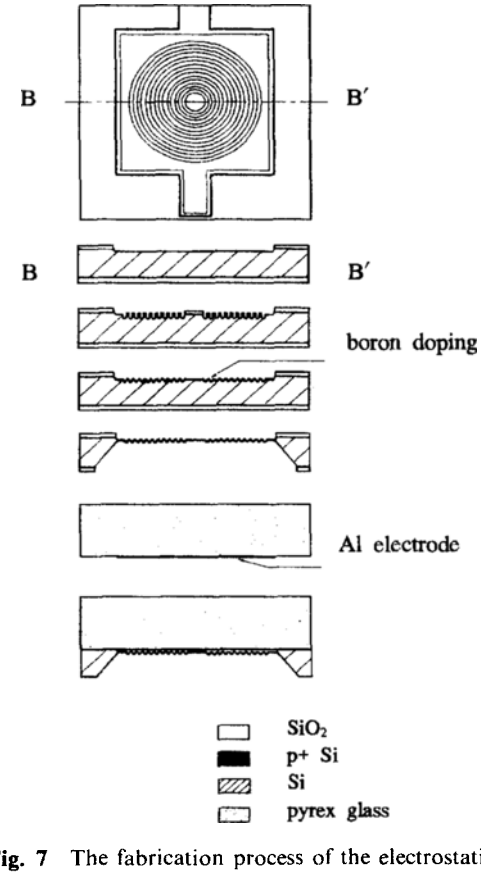

Fig. 7 The fabrication process of the electrostatic actuator with the corrugated diaphragm.

(a) The backside of the flat diaphragm

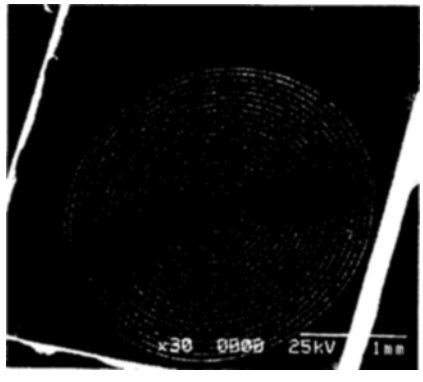

(b) The backside of the corrugated diaphragm

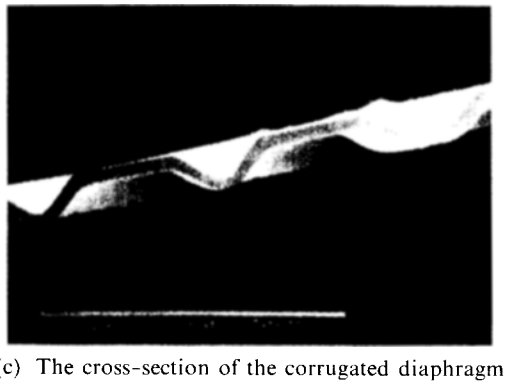

(c) The cross-section of the corrugated diaphragm

Fig. 8 The SEM photograph of the fabricated diaphragm.

diaphragm with a large initial stress. In this paper, Eq. (2) is used for the estimation of the static deflection of the flat diaphragm.

3. Fabrication Process

Figures 6 and 7 show the fabrication processes of the diaphragms actuated electrostatically. The starting material used is double side polished n-type (100) silicon wafer of 450 μm in thickness. Initially, 0.8 μm thick oxide for etch mask is thermally grown. For the fabrication of the space between the two counter electrodes, the frontside of the wafer is etched with EPW (Ethylendiamine: Pyrocatechol: DI water=250 ml : 40 g: 80 ml) solution at 115±2℃ by 9 μm. After the residual oxide is etched off, 0.5 μm thick thermal oxide is grown again. In order to fabricate the corrugated diaphragm, the silicon wafer is patterned and etched by 14 μm with EPW to form concentric circular corrugations, whereas the wafer for the flat one is not etched. To make a reference for the double side alignment, a hole is etched through the wafer with EPW etchant. Boron is diffused into the flat and the corrugated surfaces to make p^+ etch stop layers. The diffusion is performed with BN1100 solid source in N_2 ambient gas at 1100℃ for 10 hours. After removal of BSG layer, the drive-in process for 1 hour at 1000℃ is followed by patterning for the backside etch of the wafer. The backside of the wafer is etched with EPW to fabricate the diaphragms. The surface of p^+ layer of the frontside is etched for 30 minutes to avoid the possibility of buckling of the diaphragm. Figures 8(a) ~ (c) are the SEM photographs of the fabricated p^+ diaphragms. In order to construct the counter electrodes, the processed silicon wafer is anodically bonded with a #7740 pyrex glass on which aluminium electrode is deposited. The anodic bonding is performed at 300℃ with an applied voltage of 800V. During the bonding, the space between the two electrodes is not sealed to prevent the diaphragm from swelling due to the expansion of the gas in the cavity.

4. Results and Discussions

Figure 9 shows the block diagram of the measurement system. AC sinusoidal voltage is applied between the two electrodes of the fabricated actuators. The dynamic characteristics of the fabricated actuators are obtained by measuring the velocity of the center of the diaphragm using

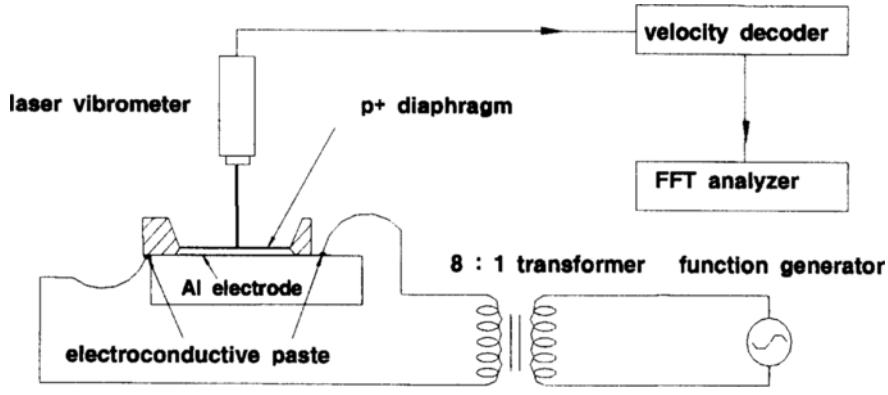

Fig. 9 The block diagram of the measurement system.

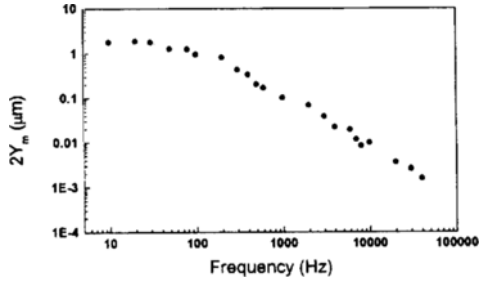

Fig. 10 The frequency response of the flat diaphragm for the input voltage of 45 V.

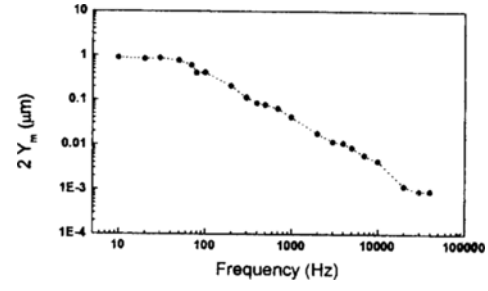

Fig. 11 The frequency response of the corrugated diaphragm for the input voltage of 45 V.

a laser vibrometer (Polytec OFV352 laser head with OFV2600 controller). The spot size is 300 μm, and the dimension of the diaphragm is 3×3 mm^2. Especially, in the case of the corrugated diaphragm, the diameter of the flat center zone for the deflection measurement is about 380 μm. The velocity amplitude is measured by an FFT analyzer (Lecroy 9310 dual oscilloscope).

If the deflection is negligibly small compared to the electrode gap, the electrostatic force is approximately propotional to V^2 as in Eq. (1). When $V = V_m \cos \omega t$,

$$V^2=\frac{V_m^2}{2}(1+\cos 2\omega t) \tag{6}$$

and the deflection, y is expected to be

$$y= Y_m(0) + Y_m(2\omega)[\cos(2\omega t+\psi(2\omega))] \tag{7}$$

where $Y_m(2\omega)$ and $\psi(2\omega)$ are the amplitude and the phase of the deflection at the frequency of 2ω, respectively. The deflection amplitude can be obtained from the velocity amplitude, $V_o(2\omega)$ measured at the frequency of 2ω by means of the FFT analyzer.

$$Y_m(2\omega)=\frac{V_o(2\omega)}{2\omega} \tag{8}$$

As the frequency approaches zero, the velocity amplitude goes to zero. However, the deflection amplitude at the frequency below the corner frequency is $Y_m(0)$. If ω approaches zero in Eq. (7), the deflection, y becomes $2Y_m(0)$, which is the static deflection to DC input voltage of V_m.

Figures 10 and 11 illustrate the measured frequency responses of the peak-to-peak deflection, $2Y_m$ of the flat and the corrugated diaphragms, respectively, when the input voltage amplitude is 45 V. The static deflections of the flat and the corrugated diaphragms are 1.7 μm and 0.88 μm, respectively. The measured values of the two diaphragms do not coincide with the estimated deflections under the residual stress of 20 MPa. In the case of the flat diaphragms, the difference is due mainly to the residual stress. The residual

stress can be determined from the comparison of the measured deflection and the deflection estimated under various residual stresses for flat diaphragm. In order to calculate the electrostatic force closer to the real value, half the center deflection is regarded as the equivalent deflection of the overall convex diaphragm. Figures 12 and 13 show the typical force-deflection curves for the flat and the corrugated p^+ diaphragms with various residual stresses, respectively. If the residual stress is 12 MPa, the deflection of the flat diaphragms coincides with the measurement deflection, 1.7 μm. The estimated static deflection of the corrugated diaphragm with the residual stress of 12 MPa is 2.5 μm. The measurement results and estimated data are summarized in Table 2.

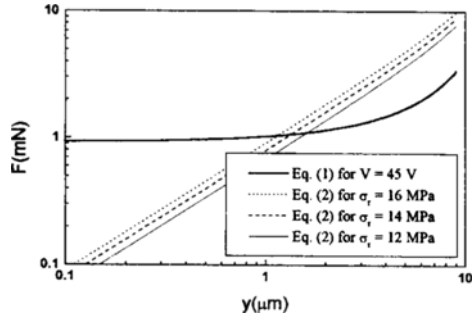

Fig. 12 The center deflection of the flat diaphragm vs. the electrostatic force.

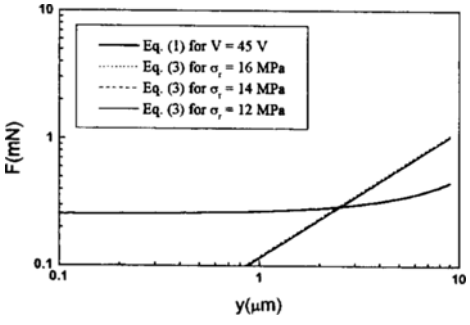

Fig. 13 The center deflection of the corrugated diaphragm vs. the electrostatic force.

As shown in Fig. 13, the static deflection of the corrugated diaphragm is not so sensitive to the residual stress as the flat one. The difference between the measured and the calculated values for the corrugated diaphragm is not exactly analyzed in this paper. There are several possible reasons for the difference. One is attributed to the approximation in the calculation of the electrostatic force. The electrostatic force was calculated under the assumption that a virtual flat electrode instead of the corrugated diaphragm is located at the center of the corrugation. Accurate calculation of the electrostatic force between the corrugated diaphragm and the flat electrode is beyond the scope of this study. Another is attributed to the simple use of Eq. (3). Equation (3) is effective under the assumption that the residual stress distribution is uniform and tensile through the depth of the diaphragm which is not true according to the previous work (Yang and Yang, 1996). In addition to that, the shape and the corrugation profile of the fabricated diaphragm are different from those in the calculation because of the flat center zone and the anisotropic characteristic of the etchant to the silicon. Each of these causes some error in calculating the diaphragm deflection and may be superposed to make the difference.

As shown in Figs. 10 and 11, both the flat and the corrugated diaphragms have the same first -order dynamics. The corner frequencies of the flat and the corrugated diaphragms are 40 Hz and 60 Hz, respectively. The deflection decay in the

Table 2 The measured and the calculated deflections for the flat and the corrugated diaphragms.

	Flat	Corrugated
Corner frequency	40 Hz	60 Hz
$2Y_m$ (measured)	1.7 μm at 10 Hz	0.88 μm at 10 Hz
Static deflection (calculated)	1.7 μm under residual stress of 12 MPa	2.5 μm under residual stress of 12 MPa

frequency greater than the corner frequency is due to the air damping. Since the chamber between the electrodes is connected to the ambient air through a narrow channel between the glass and the silicon wafer, the damping results mainly from the viscous friction in the channel when the diaphragm vibrates.

5. Conclusions

Two electrostatic actuators with p^+ diaphragms as moving electrodes have been fabricated, and the dynamic test by electrostatic actuation has been performed. One actuator has the corrugated diaphragm and the other has the flat diaphragm. According to the calculation, the deflection of the corrugated diaphragm is much larger than that of the flat one if the uniform and tensile residual stress exists in the diaphragms. For the corrugated diaphragm, the static deflection obtained from the experiment is 35 percent of the calculated value. The difference between the measured and the calculated values is due mainly to the error in the calculation of the electrostatic force generated between the corrugated and the flat electrodes and the error in the use of Eq. (3). The experimental results show that both diaphragms have almost the same first-order dynamics due to the viscous damping. From the experimental and the calculation results, it is confirmed that the corrugated diaphragm is not adequate for electrostatic applications and the flat one is preferable.

References

Ding, X. and Ko, W. H., 1991, "Buckling Behavior of Boron doped p^+ Silicon Diaphragms," *Tech. Digest, IEEE Transducers '91*, pp. 93~96.

Ding, X., Ko, W. H. and Mansour, J. M., 1989, "Residual Stress and Mechanical Properties of Boron doped p^+ Silicon Films," *Proc., IEEE Transducers '89*, Vol. 2, pp. 866~871.

Hamberg, M. W., Neagu, C., Gardeniers, J. G. E., Jntema, D. J. I. and Elwenspoek, M., 1995, "An Electrochemical Micro Actuator," *IEEE Microelectromecanical Systems Workshop*, pp. 106~110.

Jerman, J. H., 1989, "The Fabrication and Use of Micromachined Corrugated Silicon Diaphragms," *Proc., IEEE Transducers '89*, Vol. 2, pp. 988~992.

Maseeh, F. and Senturia, S. D., 1989, "Plastic Deformation of Highly Doped Silicon," *Proc., IEEE Transducers '89*, Vol. 2, pp. 861~865.

Mullem, C. J., Gabriel, K. J. and Fujita, H., 1991, "Large Deflection Performance of Surface Micromachined Corrugated Diaphragms," *Tech. Digest, IEEE Transducers '91*, pp. 1014~1017.

Scheeper, P. R., Olthuis, W. and Bergveld, P., 1994, "The Design, Fabrication, and Testing of Corrugated Silicon Nitride Diaphragms," *Journal of Microelectromechanical Systems*, Vol. 3, pp. 36~42.

Spiering, V. L., Bouwstra, S., Spiering, R. M. E. J. and Elwenspoek, M., 1991, "On-Chip Decoupling Zone for Package-stress reduction," *Tech. Digest, IEEE Transducers '91*, pp. 982~985.

Wilner, L. B., 1992, "Strain and Strain Relief in Highly Doped Silicon," *IEEE Solid-State Sensor and Actuator Workshop*, pp. 76~77.

Yang, E. H. and Yang, S. S., 1996, "The Quantitative Determination of the Residual Stress Profile in Oxidized p+ Silicon Films," *Sensors and Actuators A*, Vol. 54, pp. 684~689.

Zhang, Y. and Wise, K. D., 1993, "Performance of Non-Planar Silicon Diaphragms under Large Deflections," *IEEE Microelectromecanical Systems Workshop*, pp. 284~288.